Capillary-Induced Phase Separation in Mixed Polymer Solutions. A Lattice Mean-Field Calculation Study

Fredrik Joabsson[†] and Per Linse*

Department of Physical Chemistry 1, Center for Chemistry and Chemical Engineering, Lund University, P.O. Box 124, S-221 00 Lund, Sweden

Received: August 17, 2001; In Final Form: January 18, 2002

The formation of a capillary phase in segregating mixed polymer solutions confined between two planar walls is modeled by using a lattice mean-field theory for flexible polymers in solution. A capillary-induced phase separation (CIPS) may appear in systems where the two polymer components display different preference for the wall, the preference being either of energetic or entropic origin. A long-range attractive force operating between the walls across the polymer solution is associated with the CIPS. The CIPS phenomenon is discussed for two different polymer systems. The effects of the chain length asymmetry, the solution composition, and the interactions with the walls on the range and the magnitude of the attractive force are presented. For compositions near the binodal curve and far from the critical point, the attractive force is very long-ranged and its range exceeds far the dimension of the polymer chains. Polymer distributions between the walls at the onset of the attractive force in the systems are also reported.

Introduction

The stability of colloidal particle dispersions containing dissolved polymers is of general interest in both basic science and technical applications. It has recently been found that in polymer solutions that are near phase separation, a long-ranged attractive force may arise between surfaces and as a consequence, dispersed particles may flocculate.[1−3] The mechanism behind the attraction was attributed to a capillary-induced phase separation (CIPS), which constitutes a new destabilization mechanism to the already diverse field of polymer-mediated forces between colloidal objects.[4]

The basic physics behind the CIPS mechanism is the well-known phenomenon of capillary condensation.[5] The formation of a capillary phase is driven by a lower interfacial free energy of the capillary phase/solid interface as compared to the solution (reservoir) phase/solid interface. This is opposed by the higher free energy density of the capillary phase as compared to the reservoir phase. Moreover, the free energy of the capillary phase reduces as the surface separation is reduced due to a reduction of the volume of the capillary phase and a smaller interfacial area between the capillary and reservoir phases. As a consequence, an attractive force between the surfaces appears as soon as the free energy balance favors the formation of a capillary phase.

Previous experimental investigations have proved the existence of the CIPS force in the well characterized poly(ethylene oxide)/dextran/water system,[2,3] as well as in quasi-binary aqueous polymer solutions of polydisperse ethyl(hydroxyethyl)-cellulose.[1] In these systems, this force can be very long-ranged − of the order of 100 nm or larger.[1,2]

Capillary-induced phase separation is a well-known and very general phenomenon. It is not only restricted to mixed polymer solutions, other related examples involve colloidal particle aggregation in mixed solvents[6,7] and in polymer blends,[8] as well as protein aggregation in biological membranes.[9,10] In 1985, Beysens and Estève made the first observation of particle flocculation in a binary solvent.[6] They found flocculation of silica particles close to the binodal curve of the water/lutidine system, and interpreted the flocculation as caused by a prewetting transition that can occur in the vicinity of the binodal curve. This would lead to a particle aggregation due to an effective attraction between the particles originating from the enthalpic gain of sharing the wetting phase among two or more particles, i.e., a capillary-induced phase separation and a subsequent flocculation of the particles. The discovery by Beysens and Estève has been followed by several experimental[6,7,11−19] and theoretical[9,10,20,21] studies on the same theme.

An analytic description of the CIPS has previously been presented.[2] In the present paper, we extend the theoretical examination of the CIPS phenomenon in mixed polymer solutions by means of a lattice mean-field theory. The aim of our study is to provide further theoretical support of the CIPS phenomenon and to examine characteristic features of it as a function of various system parameters.

Theoretical Approach

Lattice Mean-Field Theory. The Flory−Huggins lattice theory of homogeneous polymer solutions[22] has been extended by Scheutjens and Fleer[23,24] to describe the adsorption and interfacial properties of flexible polymers at solid surfaces. We are applying this theory to examine systems consisting of two parallel impenetrable walls separated by a polymer solution containing two types of polymers.

The space between the walls is divided into layers parallel to the surfaces of the walls, and the layers are numbered $i = 1, 2, ..., D$ starting form the layer adjacent to one of the surfaces. Each layer is further divided into lattice sites of equal size, and each site can host either a polymer segment or solvent. Within each layer the Bragg-Williams approximation of random mixing

* To whom correspondence should be addressed. E-mail: *per.linse@fkem1.lu.se*, fax: +46 46 222 44 13.

[†] Present address: Camurus AB, Ideon Gamma 2, Sölvegatan 41, S-223 70 Lund, Sweden.

10.1021/jp013199q CCC: $22.00
Published on Web 03/23/2002

is applied, and thus, all lattice sites in a layer are equivalent. A hexagonal, closed-packed structure has been adopted, which implies that the number of nearest-neighbor sites, z, is 12. The lattice is completely filled by the polymer solution containing polymer 1 (P_1), polymer 2 (P_2), and solvent (S). The system contains n_x molecules of component x, and each molecule consists of r_x segments ($r_{P1} \gg 1$, $r_{P2} \gg 1$, and $r_S = 1$). The nature of the polymer segments, the solvent, and the walls are referred to as species.

The polymer conformations, and thus the segment spatial distribution, are affected by the presence of the surfaces. Various conformations of the polymer chains can be distinguished according to the different ordering of their segments with respect to the layer numbers. A conformation c of component x is defined as a sequence of layer numbers denoting in which layer each segment resides. With this definition, and neglecting self-exclusion, the degeneration of a conformation c of component x becomes $\exp[(r_x - 1)\ln z + \ln \omega_{xc}]$. The factor, ω_{xc}, is a product of the number of sites in the layer where the first segment is located and of λ_{ij} factors, one for each segment except the first, which gives the probability of arranging the segments according to conformation c. λ_{ij} denotes the fraction of nearest-neighbor sites in layer j viewed from a site in layer i.

To derive expressions for the segment distribution, we need to know how the (Helmholtz) free energy depends on the system parameters. Starting from the partition function of the model system, the free energy of the system relative to the reference state (designated with *) of separated amorphous components may be expressed as

$$\beta(A - A^*) = -\ln \frac{\Omega}{\Omega^*} + \beta(U - U^*) \tag{1}$$

where $\beta = 1/(kT)$, k being the Boltzmann constant and T the absolute temperature. The first term on the right-hand side of eq 1 denotes the mixing entropy and the second one the mixing energy of the system.

When the self-exclusion on a mean-field level is taken into account and the contributions from all conformations of all the components are included, the total conformational degeneration relative to the amorphous reference state, constituting the mixing entropy of the system, is given by[25]

$$\ln \frac{\Omega}{\Omega^*} = -\sum_x \sum_c n_{xc} \ln \frac{n_{xc} r_x}{\omega_{xc}} \tag{2}$$

where n_{xc} denotes the number of chains of component x in conformation c.

The only interactions considered in the system are between adjacent lattice sites, which is described by Flory−Huggins χ-parameters. The same description is used for the interaction between a polymer segment or solvent with a wall. Summing up all these interactions, the interaction energy can be expressed as

$$\beta U = \frac{1}{2} L \sum_{i=0}^{D+1} \sum_{A}^{w} \sum_{A'}^{w} \phi_{Ai} \chi_{AA'} \langle \phi_{A'i} \rangle \tag{3}$$

where L denotes the number of lattice sites in a layer, $\sum_A^w$ a sum over all species including that of the wall, and $<...>$ an average over the actual and adjacent layers according to $<x_i> = \lambda_{i,i-1}x_{i-1} + \lambda_{i,i}x_i + \lambda_{i,i+1}x_{i+1}$.

Minimization of the free energy with respect to the set $\{n_{xc}\}$ and the use of the packing constrain results in an expression for the layer-dependent species potential u_{Ai}, which denotes the relative free energy of an unconnected segment A located in a layer i. The species potential can be divided into two parts, one species independent, u'_i, and the other dependent on the species, u_{Ai}^{int}, according to

$$u_{Ai} = u'_i + u_{Ai}^{int} \tag{4}$$

If the species potentials are defined with respect to the bulk solution, i.e., if $u_A^b = 0$, then the two terms are given by

$$\beta u'_i \equiv \alpha_i + \sum_x \frac{\phi_x^b}{r_x} + \frac{1}{2} \sum_{A'} \sum_{A''} \phi_{A'}^b \chi_{A'A''} \phi_{A''}^b$$

$$\beta u_{Ai}^{int} \equiv \sum_{A'}^{w} \chi_{AA'} (<\phi_{A'i}> - \phi_{A'}^b) \tag{5}$$

The species-independent potential u'_i, which is related to the lateral pressure in a continuous model, ensures that by a suitable choice of α_i the space is completely filled in layer i. In bulk, u' becomes zero. The species-dependent term u_{Ai}^{int} consists of the mixing energy for species A in layer i being diminished by the mixing energy for species A in bulk. At distances far from the surface, ϕ_{Ai} approaches ϕ_A^b, and hence, u_{Ai}^{int} becomes zero.

The second aspect of determining the segment distribution is to take into account the chain connectivity. If only monomers are present, the volume fraction ϕ_{Ai} of monomer A in layer i is related to the bulk volume fraction ϕ_A^b according to

$$\phi_{Ai} = G_{Ai} \phi_A^b \tag{6}$$

where the weighting factor G_{Ai} for species A in layer i is given by

$$G_{Ai} = e^{-\beta u_{Ai}} \tag{7}$$

For polymers a more complex approach has to be taken. However, by use of a matrix method, the segment distribution as expressed in terms of n_{xsi}, the number of sites in layer i occupied by segments of rank s belonging to component x, is given by[25]

$$n_{xsi} = C_x \{\Delta_i^T \cdot [\prod_{s'=r_x}^{s+1} (\mathbf{W}^{t(x,s')})^T] \cdot \mathbf{s}\} \{\Delta_i^T \cdot [\prod_{s'=2}^{s} \mathbf{W}^{t(x,s')}] \cdot \mathbf{p}(x,1)\} \tag{8}$$

where C_x is a normalization factor (related to the amount of or to the bulk volume fraction of component x), $\mathbf{W}^{t(x,s)}$ a tridiagonal matrix comprising elements that contain factors describing the lattice topology and weighting factors for the segment of rank s belonging to component x, and $\mathbf{p}(x,1)$ a vector describing the distribution of the first segment of component x in the layers, with Δ and $\mathbf{s}$ being elementary column vectors. From n_{xsi} the segment volume fractions are easily be obtained. The species volume fraction ϕ_{Ai} is given by

$$\phi_{Ai} = \frac{1}{L_i} \sum_x \sum_{s=1}^{r_s} \delta_{A,t(x,s)} n_{xsi} \tag{9}$$

where the Kronecker δ only selects segments of rank s of component x if they are of type A. Thus, given the species

TABLE 1: Parameters of the Systems

quantity	symmetric system	asymmetric system
degree of polymerization	$r_{P1} = 1000$ $r_{P2} = 1000$ $r_S = 1$	$r_{P1} = 100$ $r_{P2} = 1000$ $r_S = 1$
solution interaction parameters	$\chi_{P1-S} = 0.4$ $\chi_{P2-S} = 0.4$ $\chi_{P1-P2} = 0.0188$	$\chi_{P1-S} = 0.4$ $\chi_{P2-S} = 0.4$ $\chi_{P1-P2} = 0.08$
wall interaction parameters[a]	$\Delta\chi_{P1} = -0.4, -0.8$ $\Delta\chi_{P2} = 0$	$\Delta\chi_{P1} = 0, -0.2, -0.4, -0.8$ $\Delta\chi_{P2} = 0$

[a] $\Delta\chi_{P1} \equiv \chi_{P1-w} - \chi_{S-w}$ and $\Delta\chi_{P2} \equiv \chi_{P2-w} - \chi_{S-w}$.

potentials u_{Ai}, the species volume profiles ϕ_{Ai} are obtained by eqs 7−9, these equations together with eqs 4 and 5 constituting an implicit set of nonlinear equations for the segment distributions. Finally, the excess surface free energy of the system can be expressed as

$$A^\sigma = (A - A^*) - \sum_x n_x(\mu_x - \mu_x^*) \tag{10}$$

where the sum extends over the components of the system that are in equilibrium with the bulk solution and where μ_x denotes the chemical potential of component x.

Polymer Systems. Two ternary $P_1/P_2/S$ systems confined between the two impenetrable walls have been modeled. In one system, the two polymers are of equal length $r_{P1} = r_{P2} = 1000$ (symmetric system), whereas in the other one $r_{P1} = 100$ and $r_{P2} = 1000$ (asymmetric system) have been used. In both systems, the polymers are dissolved in a good solvent. The polymer 1-polymer 2 interaction parameters, χ_{P1-P2}, were chosen to give critical points at $\phi_S \approx 0.90$ in both systems. There are three interaction parameters involving the wall, viz. χ_{P1-w}, χ_{P2-w}, and χ_{S-w}, but only their differences play a physical role. Therefore, we introduce $\Delta\chi_{P1} \equiv \chi_{P1-w} - \chi_{S-w}$ and similar for $\Delta\chi_{P2}$, where hence, e.g., $\Delta\chi_{P1} < 0$ means that the surface energetically prefer polymer 1 over the solvent. Throughout, $\Delta\chi_{P2} = 0$ and most often $\Delta\chi_{P1} < 0$ have been used also implying that polymer 1 has a more favorable interaction with the walls as compared to polymer 2. All parameters for the two systems are compiled in Table 1.

Capillary-Induced Phase and Forces. For a polymer solution between two nearby walls in full equilibrium with a reservoir near a segregative phase separation, two locally stable numerical solutions of the model may exist. One is the adiabatic continuation of the numerical solution appearing at large wall separations, and this numerical solution will be referred to as "res" (for reservoir). The other numerical solution corresponds to a capillary-induced phase in the gap between the walls, and it will be referred to as "cap".

The difference of the excess surface free energies between the two numerical solutions at separation D is defined according to

$$\Delta A^\sigma(D) \equiv A^\sigma_{cap}(D) - A^\sigma_{res}(D) \tag{11}$$

and moreover the distance at which $\Delta A^\sigma(D) = 0$ is denoted by $D = D_{onset}$. Note, both $A^\sigma_{cap}(D)$ and $A^\sigma_{res}(D)$ are excess free energies with respect to the *reservoir*. At wall separations smaller than D_{onset}, $\Delta A^\sigma < 0$ and the capillary phase is stable and the reservoir one metastable, while at separations larger than D_{onset} the reservoir phase is stable and the capillary one metastable. Thus, D_{onset} is the largest separation at which the capillary phase is stable. Typical behavior of $A^\sigma_{cap}(D)$ and $A^\sigma_{res}(D)$ as a function of D and the crossing of these functions are shown in Figure 1.

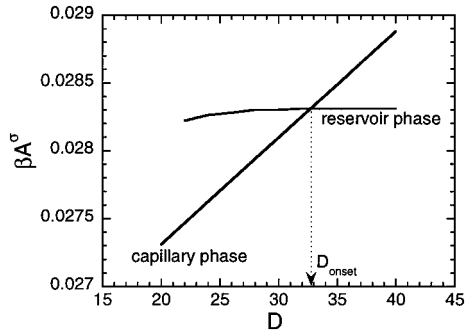

Figure 1. Typical reduced excess surface free energy (βA^σ) for the capillary and reservoir phases vs the wall separation (D) for a reservoir composition near the binodal curve. The capillary phase is stable at short D, and D_{onset} is defined as the largest wall separation at which the capillary phase remains stable.

Finally, the force operating between the walls is readily available according to

$$F(D) = -\frac{\partial A^\sigma(D)}{\partial D} \approx -\frac{1}{2}[A^\sigma(D+1) - A^\sigma(D-1)] \tag{12}$$

where A^σ is either A^σ_{cap} or A^σ_{res}.

Results

Phase Diagram. The phase diagrams of the two polymer solutions considered are given in Figure 2. Above the binodal curves and near the solvent corner, the systems display stable one-phase regions, whereas at higher total polymer concentration two-phase regions appear. Typical tie-lines connecting phases being in equilibrium are also displayed. In the symmetric system, the binodal curve is symmetric with respect to the two polymers and the tie-lines are parallel with the P_1/P_2-axis, whereas in the asymmetric system, the binodal curve is shifted toward the P_1/S-axis and the tie-lines are not parallel to the P_1/P_2-axis any more. The extension of the two-phase region in the direction to the solvent corner is mainly determined by χ_{P1-P2}, and the selected values for the two systems give nearly the same solvent volume fraction at the critical points.

From previous experience, the CIPS force is known to appear only near the binodal curve and to become more prominent far from the critical point.[2,3,6] The range of the CIPS force was found to depend on many parameters, such as reservoir composition, chain length asymmetry, and wall interactions. Rather than using the conventional volume fractions to describe the composition of the ternary system, we found it more convenient to use two other independent variables. They are (i) the ratio of the volume fractions of the two polymers, $l \equiv \phi_{P1}/\phi_{P2}$, and (ii) $\Delta\phi_{S,l} \equiv \phi_{S,l} - \phi^*_{S,l}$, where $\phi_{S,l}$ denotes the solvent volume fraction at l and $\phi^*_{S,l}$ the corresponding quantity at the binodal curve. Thus, systems with same l possess the same relative amount of the polymers and are thus located on the same dilution line (dotted lines in Figure 2), whereas $\Delta\phi_{S,l}$ denotes how close the system on this particular dilution line is the bindoal curve.

Range of CIPS Force. The range of the CIPS force can be illustrated in several ways. In Figure 2, we have selected to display iso-D_{onset} curves for $\Delta\chi_{P1} = -0.4$ for different D_{onset}. Along these curves, the onset of the CIPS force appears at the same wall-wall separation, here 25, 50, 100, or 200 layers. Since the free energy of bringing a binary P_1/S solution into contact with the wall is lower than that for a binary P_2/S solution, these curves have to appear on the P_2-rich branch of the binodal curve.

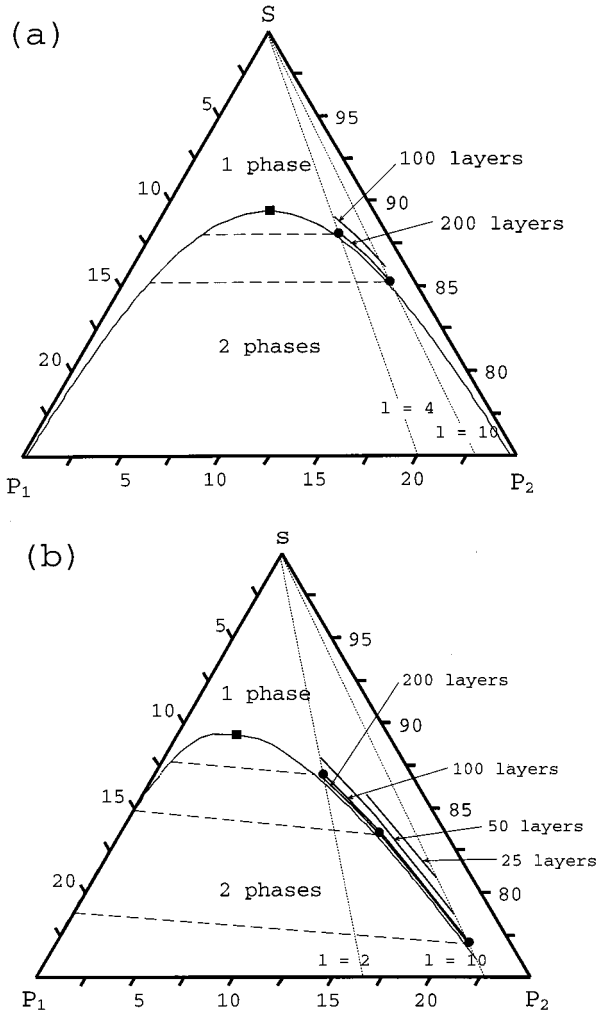

Figure 2. Binodal curves (solid curves) with critical points (squares), tie-lines (dashed lines), dilution lines at indicated values of the dilution ratio (dotted lines), and iso-D_{onset} curves at indicated values D_{onset} (solid curves) for the (a) symmetric and (b) asymmetric systems at $\Delta\chi_{P1} = -0.4$. The polymer 1-polymer 2 interaction parameters were chosen differently to give similar critical points in both systems (see also Table 1). The filled circles refer to systems considered in Figures 7−9.

As displayed in Figure 2, the model calculations show that the CIPS force appears only in a region near the binodal curves. Iso-D_{onset} curves are only given for $l \geq 4$ (symmetric system) and $l \geq 2$ (asymmetric system), due to problems of finding numerical solutions for the metastable phases closer to the critical point. We have not pushed the numerical efforts to examine the behavior of the CIPS phenomenon closer to the critical point.

Figure 3 shows for the symmetric system the onset of the attractive capillary force, D_{onset}, along the dilution lines $l = 4$ and 10 at different values of $\Delta\chi_{P1}$. Since the two types of chains possess the same degrees of polymerization and interactions with the solvent and moreover $\Delta\chi_{P2} = 0$, $\Delta\chi_{P1} < 0$ is required to have a CIPS attraction. Our numerical results showed that CIPS attraction were obtained for $\Delta\chi_{P1} = -0.4$, but not for $\Delta\chi_{P1} = -0.2$. Hence, only a weak difference between the wall-polymer interactions gives rise to a CIPS attraction. Moreover, Figure 3 shows that the onset of the attraction (i) decreases strongly with increasing distance from the binodal curve ($\Delta\phi_{S,l}$), (ii) is only weakly dependent on the ratio of the volume fractions of the two polymers (l), and (iii) is weakly dependent on the polymer 1-wall interaction ($\Delta\chi_{P1}$).

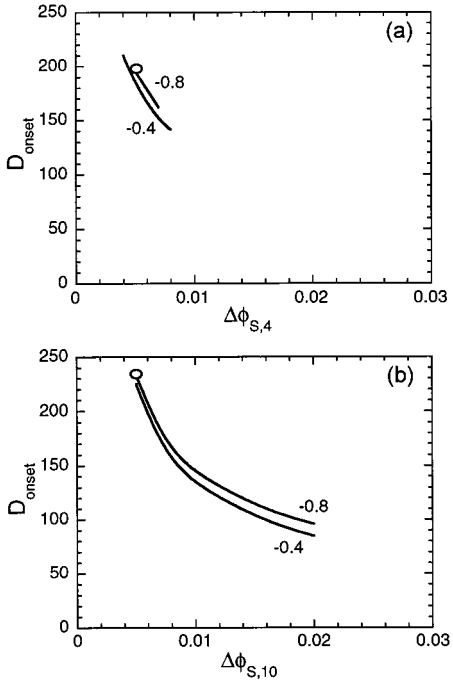

Figure 3. Onset of the capillary force (D_{onset}) vs $\Delta\phi_{S,l}$ for the symmetric system at the dilution lines (a) $l = 4$ and (b) $l = 10$ at indicated $\Delta\chi_{P1}$. The circles in (a) and (b) refer to systems considered in Figures 7a and b, respectively.

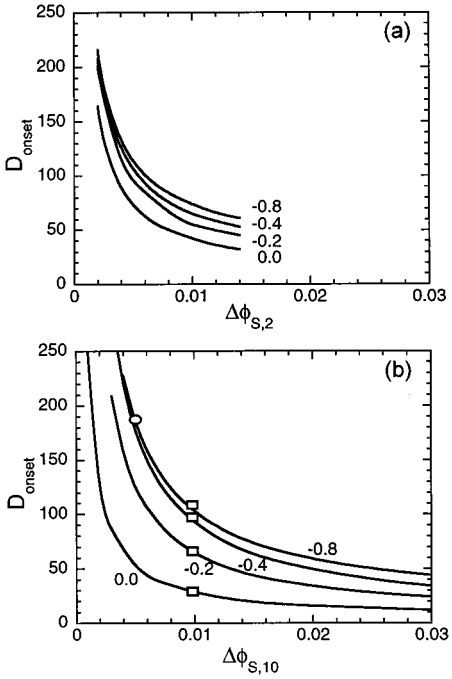

Figure 4. Onset of the capillary force (D_{onset}) vs $\Delta\phi_{S,l}$ for the asymmetric system at the dilution lines (a) $l = 2$ and (b) $l = 10$ at indicated $\Delta\chi_{P1}$. The circle and squares in (b) refer to systems considered in Figures 8b and 9, respectively.

The results of the corresponding examination of the asymmetric system are displayed in Figure 4 , and we notice a richer appearance (cf. Figures 3 and 4). First we notice that the magnitude of D_{onset} is the same for the two systems. However, most prominently and in contradiction to the symmetric system, a stable capillary phase was found for $\Delta\chi_{P1} = 0$, i.e., *none* of the solution species have a preferential energetic interaction with the wall. Since, $\chi_{P1-S} = \chi_{P2-S}$, a length difference of the polymers only is sufficient to induce a CIPS force. In fact, for

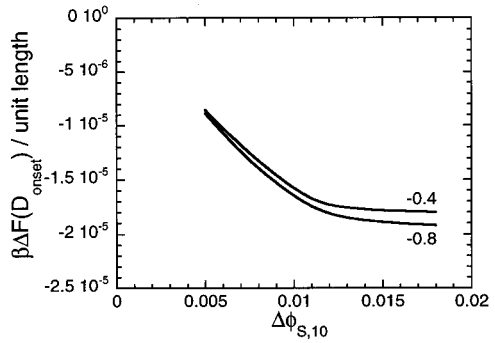

Figure 5. Reduced CIPS force at its onset $[\beta F^{\sigma}(D_{\text{onset}})]$ vs $\Delta\phi_{S,l}$ for the symmetric system at the dilution line $l = 10$ at indicated $\Delta\chi_{P1}$.

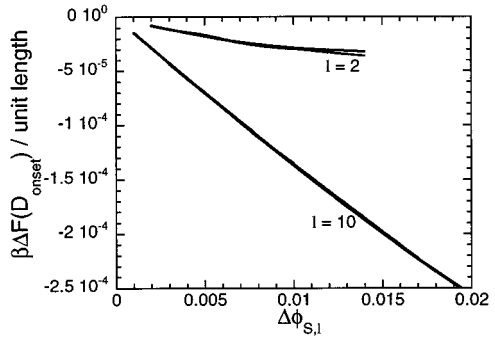

Figure 6. Reduced CIPS force at its onset $[\beta F^{\sigma}(D_{\text{onset}})]$ vs $\Delta\phi_{S,l}$ for the asymmetric system at indicated dilution lines and $\Delta\chi_{P1} = -0.8$, -0.4, -0.2, and 0.0 (most of the curves for a given dilution line overlap).

the asymmetric system CIPS appears *even* for $\Delta\chi_{P1} > 0$, e.g., at $\Delta\chi_{P1} = 0.1$ and $\Delta\phi_{S,10} = 0.003$, we obtain $D_{\text{onset}} \approx 20$.

Moreover, Figure 4 shows the asymmetric system also possesses the features that D_{onset} (i) reduces as the distance from the binodal curve is increased and (ii) is fairly insensitive on the ratio of the volume fractions of the two polymers. A difference between the systems is, however, that the range of the CIPS force in the asymmetric system is more strongly dependent on $\Delta\chi_{P1}$, a dependence which increases at lower $\Delta\chi_{P1}$ (cf. curves in, e.g., Figure 4a or b) and higher l (cf. curves in Figure 4a and b). The CIPS force becomes more long-range as $\Delta\chi_{P1}$ decreases. Moreover, for a given $\Delta\phi_{S,l}$, at $\Delta\chi_{P1} < -0.2$, the attractive force is more long-range for the dilution line $l = 2$ as compared to $l = 10$, while the opposite is found for $\Delta\chi_{P-W} > -0.2$.

Strength of CIPS Force. The present modeling is also able to predict the strength of the forces acting between the walls. According to eq 12, the constant excess surface free energy of the reservoir phase at large separation displayed in Figure 1 implies zero force acting between the walls. However, the excess surface free energy of the capillary phase is nearly linearly dependent on the wall separation with a positive slope, and hence an attractive and nearly constant CIPS force is operating. In the following, we report the force evaluated at $D = D_{\text{onset}}$ using eq 12.

For the symmetric system, Figure 5 shows that the attractive force (F negative) gets stronger as the distance to the binodal curve increases, but depends very weakly on $\Delta\chi_{P1}$. The same results hold for the asymmetric system, as shown in Figure 6. However, a comparison between the two systems for the dilution line $l = 10$ shows that the force is 1 order of magnitude stronger in the asymmetric system (cf. Figures 5 and 6). Finally, Figure 6 shows that the strength of the CIPS force reduces as the

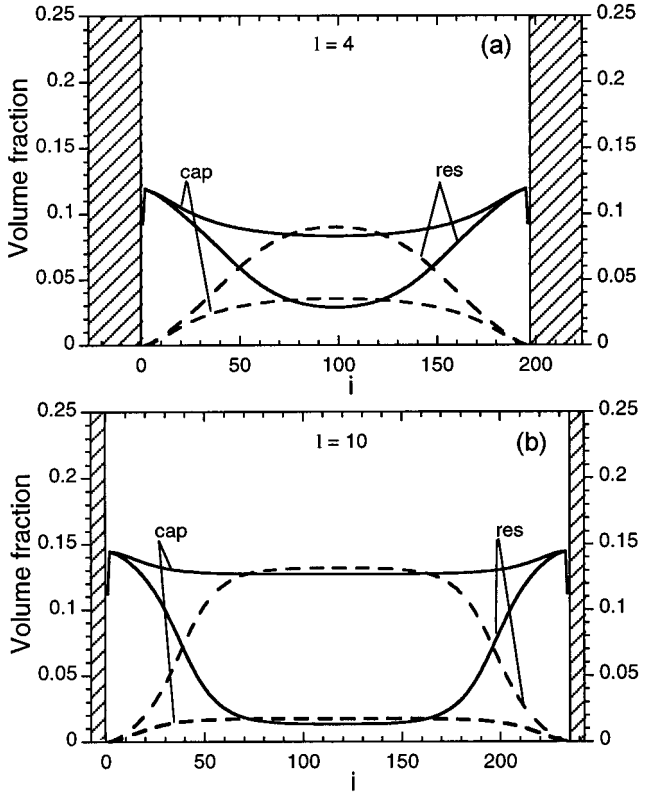

Figure 7. Polymer 1 (solid curves) and polymer 2 (dashed curves) volume fraction profiles of the coexisting capillary and reservoir phases at $D = D_{\text{onset}}$ for the symmetric system at $\Delta\chi_{P1} = -0.8$ and $\Delta\phi_S = 0.005$ at the dilution line (a) $l = 4$ corresponding to $\phi_{P1} = 0.023$ and $\phi_{P2} = 0.096$ and (b) $l = 10$ corresponding to $\phi_{P1} = 0.013$ and $\phi_{P2} = 0.132$.

binodal curve is approached (cf. the location of the dilution lines $l = 2$ and 10 in Figure 2b).

Volume Fraction Profiles. We will now consider volume fraction profiles perpendicular to the walls, which are directly obtained through eq 9. Figure 7 shows the polymer profiles of the coexisting capillary and reservoir phases at $D = D_{\text{onset}}$ for the symmetric system at $\Delta\chi_{P1} = -0.8$ and $\Delta\phi_S = 0.005$ at the dilution lines $l = 4$ and 10. The locations of the two systems in the phase diagram are displayed by the circles in Figure 2a and in the D_{onset} vs $\Delta\phi_S$ representation by the circles in Figure 3. We see that the systems are close to the binodal curve.

Starting with the reservoir phase, we find that the volume fraction in the middle of the gap approaches the bulk composition of the reservoir with $\phi_{P1} < \phi_{P2}$, whereas the volume fraction profiles closer to the walls reveal that polymer 1 is adsorbed to the walls and polymer 2 depleted from them. The adsorption of P_1 to the walls affects the layer profile ca. 60 layers out from the walls, this region being referred to as a wetting layer enriched in P_1 and depleted in P_2. Furthermore, Figure 7a displays that the wetting layers from the walls almost overlap for $l = 4$ (reservoir composition closer to the critical point), while Figure 7b shows an extended mid-gap region where the composition is almost unchanged for $l = 10$ (reservoir composition further away from the critical point). The volume fractions near the walls are similar for the two reservoir compositions considered. For the symmetric system, the different polymer volume fractions near the wall are in practice governed by their different interaction with the wall.

Regarding the capillary phases, Figure 7 shows that they are characterized by much more uniform volume fraction profiles across the gap. The volume fractions near the walls are very

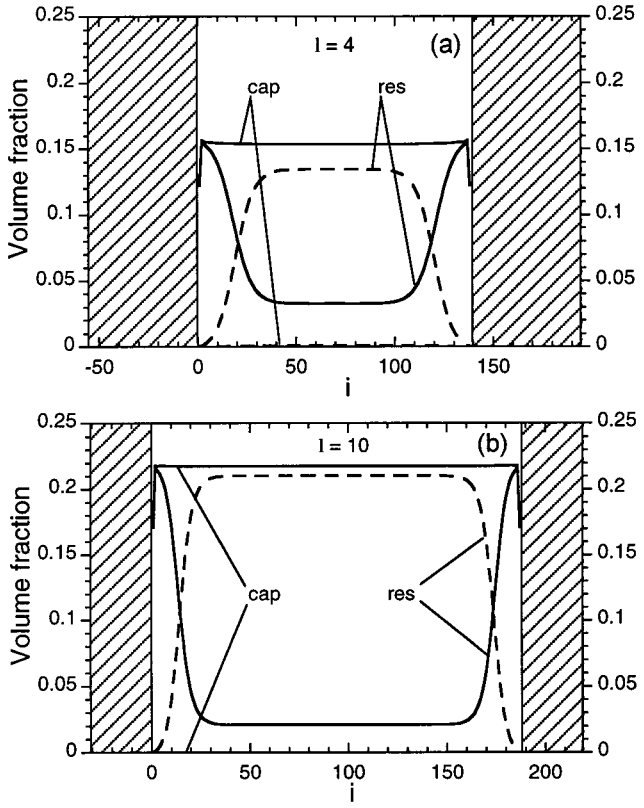

Figure 8. Polymer 1 (solid curves) and polymer 2 (dashed curves) volume fraction profiles of the coexisting capillary and reservoir phases at $D = D_{onset}$ for the asymmetric system at $\Delta\chi_{P1} = -0.8$ and $\Delta\phi_S = 0.005$ at the dilution line (a) $l = 4$ corresponding to $\phi_{P1} = 0.033$ and $\phi_{P2} = 0.134$ and (b) $l = 10$ corresponding to $\phi_{P1} = 0.021$ and $\phi_{P2} = 0.210$.

similar to those in the corresponding reservoir phases, thus they are primarily controlled by the interactions with the walls. However, the volume fractions of polymer 1 and 2 in the middle of the gap are nearly reversed as compared to the reservoir phase. A comparison with the tie-lines given in Figure 2a shows that the composition of a capillary phase is to a very good approximation given by the other end of a tie-line starting near the composition of the reservoir.

Figure 8 shows the corresponding volume fraction profiles for the asymmetric system at the dilution lines $l = 4$ and 10. The locations of the two compositions in the corresponding phase diagram are shown in Figure 2b and the location of one of them in the D_{onset} vs $\Delta\phi_S$ representation by the circle in Figure 4b. As compared to the symmetric system, the asymmetric one displays (i) much thinner wetting layers (20−30 layers), which are well separated by a mid-gap region with constant composition, and (ii) an onset of the CIPS force at shorter separation (also expressed by the smaller separation between the iso-D_{onset} curves in Figure 2). The capillary phase is enriched in polymer 1, contains very little polymer 2, and has a higher solvent content that the reservoir phase. A comparison of the capillary mid-gap volume fractions in Figure 8 with the composition at the left ends of the two lower tie-lines in Figure 2b shows again the similar composition of these phases. Thus, in concordance with what was previously found for the symmetric system, the mid-gap composition of the capillary phase correlates well with the phase diagram.

Figure 9 shows volume fraction profiles for the asymmetric system at $D = D_{onset}$, $\Delta\phi_S = 0.01$, and $l = 10$ for different values of $\Delta\chi_{P1}$. The locations of these systems are given by a single point in the phase diagram (Figure 2b) and by the

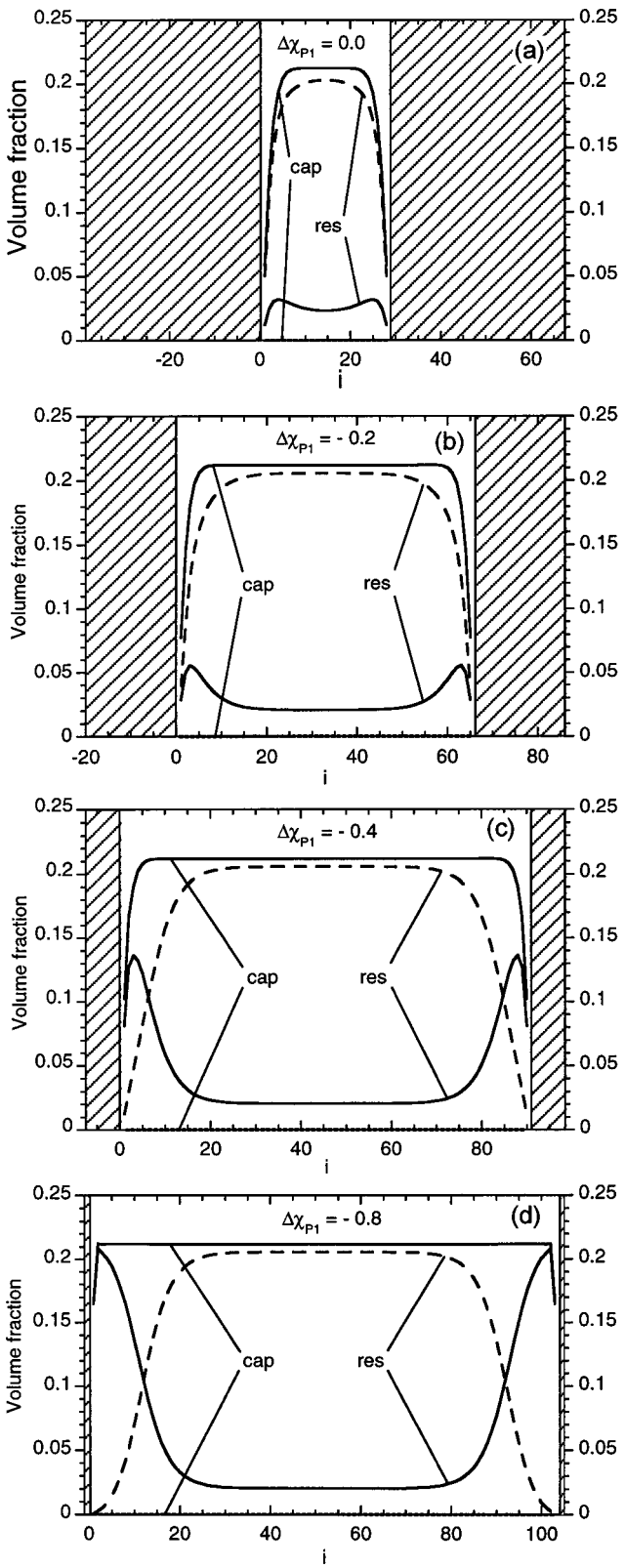

Figure 9. Polymer 1 (solid curves) and polymer 2 (dashed curves) volume fraction profiles of the coexisting capillary and reservoir phases at $D = D_{onset}$ for the asymmetric system at $\Delta\phi_S = 0.01$ and the dilution line $l = 10$ corresponding to $\phi_{P1} = 0.021$ and $\phi_{P2} = 0.206$ for (a) $\Delta\chi_{P1} = 0.0$, (b) −0.2, (c) −0.4, and (d) −0.8.

squares in the D_{onset} vs $\Delta\phi_S$ representation (Figure 4b). As the attractive interaction between polymer 1 and the wall is increased, we find that (i) the onset of the CIPS force increases from ca. 30 to 100 layers and (ii) the wetting layer of the

reservoir phase increases in thickness and becomes richer in polymer 1. For $\Delta\chi_{P1} = 0$, the wetting layers originating from the two walls nearly touch each other, whereas for lower $\Delta\chi_{P1}$ the reservoir phase displays an extended region of constant composition between the walls. Regarding the capillary phase rich in polymer 1, polymer 1 is at $\Delta\chi_{P1} = 0$ considerably depleted from the walls. Thus, the capillary phase is not formed due to the fact that the polymer 1-rich solution interacts favorably with the wall, but rather that it interacts *less* unfavorably than the polymer 2-rich solution.

Discussion

General. The excess surface free energies of the capillary and reservoir phases between the walls were in eq 11 given with respect to the composition of the reservoir. If A^{σ}_{cap} is expressed with respect to the composition of the bulk of the capillary phase, which is achieved in the middle of the gap between the two walls at large separations, we have

$$\begin{aligned}\Delta A^{\sigma}(D) &= A^{\sigma}_{cap}(D) - A^{\sigma}_{res}(D) \\ &= [A^{\sigma'}_{cap}(D) + Area^{*}D(g_{cap} - g_{res})] - A_{res}{}^{\sigma}(D) \\ &= Area^{*}\{[\gamma_{cap} + \Delta\gamma_{cap}(D) - \gamma_{res} - \Delta\gamma_{cap}(D)] + \\ &\qquad D(g_{cap} - g_{res})\} \quad (13)\end{aligned}$$

where γ_α is the surface tension of the phase α/solid interface, $\Delta\gamma_\alpha \equiv A^{\sigma}(D)/Area - \gamma_\alpha$, the change of the surface tension when bringing the surfaces from infinite distance to D, and g_α the free energy per unit volume of phase α.

In the large wall separation limit, where the volume fractions profiles at the two walls are unperturbed, $\Delta\gamma_\alpha \rightarrow 0$ and we have

$$\Delta A^{\sigma}(D) = Area^{*}[(\gamma_{cap} - \gamma_{res}) + D(g_{cap} - g_{res})] \quad (14)$$

Since the free energy per unit volume is larger in the capillary phase as compared to the reservoir phase ($g_{cap} - g_{res} > 0$), a lower surface tension of the capillary phase/solid interface as compared to the reservoir phase/solid one ($\gamma_{cap} - \gamma_{res} < 0$) is needed for the appearance of CIPS. From eq 14 and $A^{\sigma}(D) = 0$, the onset of the CIPS force appears at

$$D_{onset} = -(\gamma_{cap} - \gamma_{res})/(g_{cap} - g_{res}) \quad (15)$$

and the CIPS force becomes

$$F(D) = -(g_{cap} - g_{res}) \quad (16)$$

which is independent of the wall separation D.

This analytic analysis becomes in the large wall separation limit identical to that previously reported[2] and explains (i) the appearance of a capillary phase and (ii) the associated linear and attractive force appearing at large separation. The present numerical investigation fully supports this view and, in addition, provides a prediction on how the characteristic features of the CIPS phenomenon depends on molecular and interaction parameters and the behavior at short wall separations where $\Delta\gamma_\alpha \neq 0$. In the following, we will expand the discussion on the CIPS phenomenon on the basis of the results obtained from the lattice mean-field model.

Composition of Capillary Phase. All our numerical results indicates that the composition of the capillary phase (i) practically corresponds to a point on the bimodal curve and (ii) this point is located on a tie-line, which other end is very close to the composition of the reservoir. Table 2 provides additional data for the conditions applied in Figure 8a. We notice that in this case the volume fractions of the reservoir phase in the middle of the gap approaches the reservoir composition with volume fraction deviations smaller than 10^{-5}. The largest deviation of any volume fraction of the capillary phase, as compared to the nearest point on the binodal curve, is 3×10^{-4}, and that the composition of the point of the other end of the tie-line is indeed near (3×10^{-3}) that of the reservoir.

TABLE 2: Composition of Different Systems Related to the Conditions Used in Figure 8a

system	ϕ_S	ϕ_{P1}	ϕ_{P2}
reservoir	0.83308	0.03265	0.13427
reservoir phase (middle of the gap)	0.83308	0.03264	0.13428
capillary phase (middle of the gap)	0.84540	0.15355	0.00105
closest point on the binodal	0.8457	0.1536	0.0008
other end of tie-line	0.8345	0.0353	0.1301

Effect of Wall Interaction. Our results in Figures 4 and 5 show that the onset of the CIPS force increases as $\Delta\chi_{P1}$ is reduced, but the effect levels off as $\Delta\chi_{P1}$ becomes sufficiently low. A lowering of $\Delta\chi_{P1}$ corresponds to an increased wetability of the polymer 1-rich capillary phase as compared to the polymer 2-rich reservoir phase, and is expressed in eq 15 by a more negative value of $\gamma_{cap} - \gamma_{res}$. The magnitude of the CIPS force displayed in Figures 5 and 6 was found to be very insensitive to the surface interactions in agreement with eq 16, with $g_{cap} - g_{res}$ being only a solution property.

In the symmetric system, the different wetability of the two solutions is achieved by $\Delta\chi_{P1} < \Delta\chi_{P2}$. Figure 7 shows that CIPS does no appear until the attractive polymer 1-wall interaction makes the density of polymer 1 at the walls similar to that in the capillary phase. At this condition of strong polymer adsorption, the adsorbed layers at the walls are similar for the capillary and reservoir phases.

One of the most important results in this work is the evidence for a CIPS attraction in systems with *no* preferred wall interactions at all, but only a length difference of the polymers. Generally, polymers lose conformational entropy close to an impenetrable wall, and the loss increases with the length of the polymers, which creates the necessary $\gamma_{cap} - \gamma_{res} < 0$ condition. Figure 9a shows that at these conditions both phases may display depletion layers. Finally, the magnitude of the force at the same dilution line is much weaker for the symmetric system (cf. Figures 5 and 6).

Effect of Reservoir Composition. As the composition of the polymer 2-rich reservoir phase approaches the binodal curve, D_{onset} appears to diverge (Figures 3 and 4) and the CIPS force seems to approach zero (Figures 5 and 6). This behavior is readily predicted by eqs 15 and 16, respectively, with $g_{cap} - g_{res}$ being identical zero at the binodal curve.

The behavior becomes more diverse as the reservoir composition departures from the binodal curve. This is further illustrated in Figure 10, which displays the reduced excess surface free energies of the two phases for the asymmetric system at $\Delta\chi_{P1} = -0.4$ and some compositions along the dilution line $l = 10$ (cf. Figure 2b). First, the decrease of D_{onset} and increase of the capillary force F at increasing $\Delta\phi_S$ is obvious. At the largest $\Delta\phi_S = 0.080$ (i.e., $\phi_S = 0.844$ which corresponds to a composition closer to the binary S/P_2-axis than to the binodal curve), a transition still appears, now at $D_{onset} = 14$. The difference in composition of the polymer 1- and polymer 2-rich films is here small and no metastable phases were found. Moreover, no linear force at short separations is present, as appearing for compositions nearer the binodal curve. Instead, the force increases at decreasing separation and is best viewed as a depletion attraction; the free energy is reduced when removing the thin polymer 1-rich layer between the two walls.

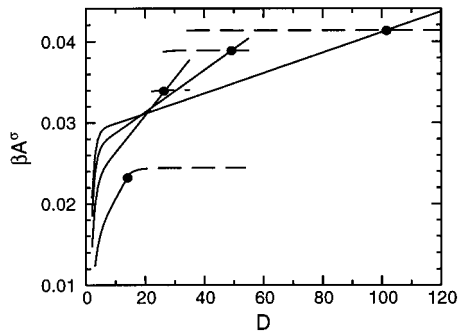

Figure 10. Reduced excess surface free energy (βA^{σ}) for the capillary (solid curves) and reservoir (dashed curves) phases vs the wall separation (D) for the asymmetric system at system at $\Delta\chi_{P1} = -0.4$ and the dilution line $l = 10$ with $\Delta\phi_S = 0.0009$, 0.0020, 0.0040, and 0.0080 (top to bottom) giving $D_{onset} \approx 100$, 50, 25, and 14 (symbols). At $\Delta\phi_S = 0.0080$, no metastable phases where found.

Finally, in those cases were no capillary phase appears at all, a conventional depletion attraction appears at short separation between the two walls.

The closeness to the critical point has been measured by employing dilution lines. Far away from the critical points, Figure 2 shows that the iso-D_{onset} curves are fairly parallel to the binodal curves indicating that $\gamma_{cap} - \gamma_{res}$ and $g_{cap} - g_{res}$ entering in eq 15 depends similarly on l. As the critical point is approached, both $\gamma_{cap} - \gamma_{res}$ and $g_{cap} - g_{res}$ approaches zero and more detailed analysis is required to determine the iso-D_{onset} curves. According to Figure 6, the CIPS force becomes reduced as the critical point is approached keeping the distance from the binodal curve (reasonably) constant. (Note, $\Delta\phi_s$ and the binodal curve are not parallel and they become less so as the critical point is approached.) Again this is directly understood from eq 16 and the fact that $g_{cap} - g_{res}$ becomes smaller along this path.

Relation to Wetting Transition. All volume fraction profiles show that the segment density is significantly altered near the walls, either showing a surface excess or depletion. Generally, when strong excess appears at a single surface, this is referred to as a formation of a wetting layer, which could appear as first-order transition. The associated attractive force, which may appear between colloids in mixed solvent or polymer solutions, is often attributed to the wetting phenomenon.[6,13,16,17,21,26]

In the present paper, we show that the attractive forces may be much more long-ranged than would be expected from a coalescence of two wetting layers. Even though wetting transitions are closely related to the CIPS phenomenon, we make a distinction and suggest that wetting transitions are better viewed as a single surface phenomenon, while CIPS requires at least two surfaces to come into play. The merge of two wetting layers corresponds to the situation when the excess free energy curve of the reservoir phase meets the corresponding curve of the capillary phase a short separation as illustrated in Figure 10 with $\Delta\phi_S = 0.0080$. At this stage, the slope of A^{σ}_{cap} is not linear and hence not given by $g_{cap} - g_{res}$ any longer.

Comparison with Experiments. Dispersions of silica in aqueous poly(ethylene oxide)/dextran solutions show flocculation far into the one-phase region, especially in the presence of small amounts of salt, which suppresses the electrostatic repulsion between the particles.[3] Our predicted results for a similarly behaving segregating polymer mixtures display qualitatively the same phase instability when the walls (representing large particles) being present. Thus, we suggest that the instability experimentally observed is caused by CIPS attraction near the binodal curve and most likely by depletion attraction further away from it.

Quasi-binary aqueous polymer solutions consisting of a polydispersed polymer and solvent also displaying CIPS[1] are also possible to model with the same approach. Such work is in progress.

Conclusions

On the basis of lattice mean-field calculations, we have demonstrated the existence of capillary-induced phase separation, CIPS, between two planar walls confining a segregating mixed polymer solution. The CIPS phenomenon was found in a narrow region close to the binodal curve on the side of the critical point, which is enriched in the component that is disfavored at the surface. In the region near the wall, a wetting layer enriched in the other component was found.

The CIPS give rise to an attractive force, due to the higher free energy density of the capillary phase. The wall separation at the onset of the force was found to be very large near the binodal, far exceeding the extension of the wetting layers. The CIPS transition was promoted by increasing the wall preference for one of the components, and by making the chain length of the two polymers asymmetric. An important result is the appearance of a CIPS attraction in systems with no preferred wall interactions at all, but only a length difference between the polymers. The shorter polymer was less disfavored at the surface and could therefore form a capillary phase.

Acknowledgment. This work was financed by the Center for Amphiphilic Polymers (CAP) and the Swedish National Research Council (NFR).

References and Notes

(1) Freyssingeas, E.; Thuresson, K.; Nylander, T.; Joabsson, F.; Lindman, B. *Langmuir* **1998**, *14*, 5877−5889.
(2) Wennerström, H.; Thuresson, K.; Linse, P.; Freyssingeas, E. *Langmuir* **1998**, *14*, 5664.
(3) Joabsson, F.; Calatayu, A.; Thuresson, K.; Piculell, L. *J. Phys. Chem. B*, submitted for publication, **2001**.
(4) Napper, D. H. *Polymeric Stabilization of Colloidal Dispersions*; Academic Press Inc.: London, 1983.
(5) Petrov, P.; Olsson, U.; Wennerström, H. *Langmuir* **1997**, *13*, 3331.
(6) Beysens, D.; Estève, D. *Phys. Rev. Lett.* **1985**, *54*, 2123.
(7) Kline, S. R.; Kaler, E. W. *Langmuir* **1994**, *10*, 412.
(8) Müller, M.; Binder, K. *Macromolecules* **1998**, *31*, 8323.
(9) Gil, T.; Ipsen, J. H. *Phys. Rev. E* **1997**, *55*, 1713.
(10) Gil, T.; Sabra, M. C.; Ipsen, J. H.; Mouritsen, O. G. *Biophys. J.* **1997**, *73*, 1728.
(11) Gallagher, P. D.; Kurnaz, M. L.; Maher, J. V. *Phys. Rev. A* **1992**, *46*, 7750.
(12) Gallagher, P. D.; Maher, J. V. *Physica A* **1991**, *177*, 489.
(13) Gurfein, V.; Beysens, D. *Phys. Rev. A* **1989**, *40*, 2543.
(14) Jayalakshmi, Y.; Kaler, E. W. *Phys. Rev. Lett.* **1997**, *78*, 1379.
(15) Koehler, R. D.; Kaler, E. W. *Langmuir* **1997**, *13*, 2463.
(16) Gurfein, V.; Perrot, F.; Beysens, D. *Prog. Colloid Polym. Sci.* **1989**, *79*, 167.
(17) van Duijneveldt, J. S.; Beysens, D. *J. Chem. Phys.* **1991**, *94*, 5222.
(18) Grüll, H.; Woermann, D. *Berichte Der Bunsen-Gesellschaft-Physical Chemistry Chemical Physics* **1997**, *101*, 814.
(19) Broide, M. L.; Garrabos, Y.; Beysens, D. *Phys. Rev. E* **1993**, *47*, 3768.
(20) Löwen, H. *Phys. Rev. Lett.* **1995**, *74*, 1028.
(21) Sluckin, T. J. *Phys. Rev. A* **1990**, *41*, 960.
(22) Flory, P. J. *Principles of Polymer Chemistry*; Cornell University Press: Ithaca, New York, 1953.
(23) Scheutjens, J. M. H. M.; Fleer, G. J.; Fleer, G. J. *J. Phys. Chem.* **1979**, *83*, 1619.
(24) Scheutjens, J. M. H. M.; Fleer, G. J. *J. Phys. Chem.* **1980**, *84*, 178.
(25) Linse, P.; Björling, M. *Macromolecules* **1991**, *24*, 6700.
(26) Beysens, D.; Petit, J. M.; Narayanan, T.; Kumar, A.; Broide, M. L. *Berichte Der Bunsen-Gesellschaft-Physical Chemistry Chemical Physics* **1994**, *98*, 382.